Available online at www.sciencedirect.com
SCIENCE DIRECT®
Physica A 353 (2005) 613–624
PHYSICA A
www.elsevier.com/locate/physa

Power-law sensitivity to initial conditions in a time series with applications to epileptic seizure detection

Jianbo Gao[a,*], Wen-wen Tung[b], Yinhe Cao[c], Jing Hu[a], Yan Qi[d]

[a]*Department of Electrical and Computer Engineering, University of Florida, Gainesville, FL 32611, USA*
[b]*National Center for Atmospheric Research, Boulder, CO 80307-3000,USA*
[c]*Biosieve, 1026 Springfield Drive, Campbell, CA 95008, USA*
[d]*Department of Biomedical Engineering, Johns Hopkins University, Baltimore, MD 21205, USA*

Received 8 November 2004
Available online 2 March 2005

Abstract

Recently, the concept of exponential sensitivity to initial conditions (ESIC) of deterministic chaos is generalized to power-law sensitivity to initial conditions (PSIC). We describe a general computational procedure to examine PSIC from a time series. Study of noise-free and noisy logistic and Henon maps at the edge of chaos finds that PSIC cannot be shown from clean scalar time series. However, when there is dynamic noise, motions around the edges of chaos all collapse onto the PSIC attractor regardless whether they are simply regular or truly chaotic when noise is absent. Hence, dynamic noise makes PSIC observable. The PSIC concept is further applied to the analysis of long continuous EEG signals with epileptic seizures. It is shown that measures from the PSIC framework is quite effective in detecting seizures, often better than the Lyapunov exponent based methods from the conventional ESIC framework.

PACS: 05.40.−a; 05.45.−a; 05.20.−y; 05.70.Ce

Keywords: Exponential sensitivity to initial conditions; Power-law sensitivity to initial conditions; Time series analysis

*Corresponding author.
E-mail address: gao@ece.ufl.edu (J. Gao).

0378-4371/$ - see front matter © 2005 Elsevier B.V. All rights reserved.
doi:10.1016/j.physa.2005.01.027

1. Introduction

The formalism of non-extensive statistical mechanics (NESM) [1] has found numerous applications to the study of systems with long-range-interactions [2–5] and multifractal behavior [6,7], and fully developed turbulence [7–9], among many others. In order to characterize a type of motion whose complexity is neither regular nor fully chaotic/random, recently the concept of exponential sensitivity to initial conditions (ESIC) of deterministic chaos has been generalized to power-law sensitivity to initial conditions (PSIC) [6,10]. Mathematically, the formulation of PSIC closely parallels that of NESM. PSIC has been applied to the study of deterministic 1-D logisticlike maps and 2-D Henon map at the edge of chaos [6,10–15], yielding considerable new insights. In this paper, we address the fundamental question of how relevant the concept of PSIC is to experimental time series analysis.

Time series analysis is an important exercise in science and engineering. One of the most important issues in time series analysis is to determine whether the data under investigation are regular, deterministically chaotic, or simply random. Along this line, a lot of work has been done in the past two decades. A bit surprisingly, often ESIC in the rigorous mathematical sense cannot be observed in experimental data. While current consensus is to attribute this fact to the noise in the data, here we show that the more general concept of PSIC provides an interesting framework for time series analysis. Specifically, by studying noise-free and noisy logistic and Henon maps at the edge of chaos, we show that when noise is absent, PSIC is hard to detect from a scalar time series. However, when there is dynamic noise, motions around the edge of chaos, be it simply regular or truly chaotic when there is no noise, all collapse onto the PSIC attractor. Hence, dynamic noise makes PSIC observable. The PSIC concept is further applied to the analysis of long continuous EEG signals with epileptic seizures. It is shown that measures from the PSIC framework is quite effective in detecting seizures.

2. General theoretical and computational framework

Throughout this paper, we shall work with scalar time series. We shall employ the Takens [16] time delay embedding to construct vectors of the form: $X_i = [x(i), x(i + L), \ldots, x(i + (m - 1)L)]$, with m the embedding dimension and L the delay time. The mapping $X_i \to X_{i+1}$ defines a dynamics. In the 1-D case, the PSIC is characterized by [6,10]

$$\xi(t) = \lim_{\Delta x(0)\to 0} \frac{\Delta x(t)}{\Delta x(0)} = [1 + (1 - q)\lambda_q t]^{1/(1-q)}, \tag{1}$$

where $\Delta x(0)$ is the infinitesimal discrepancy in the initial condition, $\Delta x(t)$ is the discrepancy at time $t > 0$, q is the entropic index, and λ_q equals K_q, the generalization of the Kolmogorov–Sinai entropy [10]. When t is large, $\xi(t) \sim t^{1/(1-q)}$. Eq. (1) is the

solution to $d\xi/dt = \lambda_q \xi^q$. When $q \to 1$, $\xi(t) \to e^{\lambda_1 t}$, which is the very definition for the ESIC.

We conjecture that Eq. (1) generalizes to high-dimensional case,

$$\xi(t) = \lim_{\|\Delta X(0)\| \to 0} \frac{\|\Delta X(t)\|}{\|\Delta X(0)\|} = [1 + (1-q)\lambda_q^{(1)} t]^{1/(1-q)}, \tag{2}$$

where $\|\Delta X(0)\|$ is the infinitesimal discrepancy between two orbits at time 0, $\|\Delta X(t)\|$ is the distance between the two orbits at time $t > 0$, q is the entropic index, and $\lambda_q^{(1)}$ is the first q-Lyapunov exponent, corresponding to the power-law increase of the first principle axis of an infinitesimal ball in the phase space [17]. $\lambda_q^{(1)}$ may not be equal to K_q. This is understood by recalling that for chaotic systems, the Kolmogorov–Sinai entropy is the sum of all the positive Lyapunov exponents (LEs). We conjecture a similar relation may hold between the q-Lyapunov exponents and K_q. Then in general, $\lambda_q^{(1)}$ may not be equal to K_q. When t is large, Eq. (2) again gives $\xi(t) \sim t^{1/(1-q)}$.

Note that under the above framework, the motion may not be like fully developed chaos, thus not ergodic [17]. In fact, recently we have shown [18] that non-stationary $1/f^\alpha$ ($1 \leqslant \alpha \leqslant 3$) processes can be characterized by PSIC, with $q = 1 - 2/(\alpha - 1)$ and $\lambda_q^{(1)} = (\alpha - 1)/2$. Indeed, in the so-called fractional Brownian motion models [19], an infinitesimal ball and its axes do increase in a power-law fashion, with the exponent being $(\alpha - 1)/2$.

Given a finite time series, the condition of $\|\Delta X(0)\| \to 0$ cannot be satisfied. In order to find the law governing the divergence of nearby orbits, one thus has to examine how the neighboring points, (X_i, X_j), in the phase space, evolve with time, by forming suitable ensemble averages. Notice that if (X_{i1}, X_{j1}) and (X_{i2}, X_{j2}) are two pairs of nearby points, when $\|X_{i1} - X_{j1}\| \ll \|X_{i2} - X_{j2}\| \ll 1$, then the separations such as $\|X_{i1+t} - X_{j1+t}\|$ and $\|X_{i2+t} - X_{j2+t}\|$ cannot be simply averaged to provide estimates for q and $\lambda_q^{(1)}$. In fact, it would be most convenient to consider ensemble averages of pairs of points (X_i, X_j) that all fall within a very thin shell, $r_1 \leqslant \|X_i - X_j\| \leqslant r_2$, where r_1 and r_2 are close. For convenience, we call r_2 and $r_2 - r_1$ the radius and the thickness of the shell, respectively. A more general computational procedure has actually been proposed in Ref. [20], for a sequence of shells. We shall comment on the effects of the shell size on $\xi(t)$ when discussing concrete examples shortly. For later convenience as well as to follow the notation of Ref. [20], we shall denote $\ln \xi(t)$ by $\Lambda(t)$. Computationally, $\Lambda(t)$ is given by

$$\ln \xi(t) \approx \Lambda(t) = \left\langle \ln\left(\frac{\|X_{i+t} - X_{j+t}\|}{\|X_i - X_j\|} \right) \right\rangle, \tag{3}$$

where the ensemble average is taken over all pairs of points (X_i, X_j) with $r_1 \leqslant \|X_i - X_j\| \leqslant r_2$, and $t > 0$ is the (discrete) evolution time, in units of the sampling time. For fully developed low-dimensional chaos, the $\Lambda(k)$ curves for different shells form a common linear envelope, for $T_a \leqslant t \leqslant T_p$ [21], with the slope of the envelope accurately estimating the largest positive Lyapunov exponent. This has been verified in well-known 1-D and higher than 1-D chaotic systems such as the Lorenz attractor, the Rossler attractor, and the Mackey–Galss delay differential equation [20]. The

existence of such a linear common envelope provides a direct dynamical test for deterministic chaos, since for random systems, such an envelope does not exist [20]. The time scale T_a is related to the time a pair of points X_i and X_j evolve to the most unstable manifold of the dynamics, and is on the order of the embedding window size, $(m-1)L$. Such a time scale usually exists for multi-dimensional systems, but not for 1-D systems. Its very existence ensures that directional mixing for chaotic systems is eliminated before the largest positive Lyapunov exponent is estimated. The time scale T_p is a prediction time scale. When $t > T_p$, the $\Lambda(k)$ curves are flat, meaning that the separation between X_{i+t} and X_{j+t} has reached some average value, determined by the diameter of the chaotic attractor. T_p is larger for smaller shells, corresponding to the fact that $\|X_{i+t} - X_{j+t}\|$ can diverge for a longer period of time before reaching the average value.

Below, we show some examples of the application of this general framework to time series analysis. In Section 3, time series generated from noise-free and noisy logistic and Henon maps will be studied. In Section 4, long continuous EEG data will be analyzed with regard to epileptic seizure detection.

3. PSIC in model systems

Let us first examine the logistic map around the edge of chaos. Considering that dynamic noise is often an important component of a system (e.g., spontaneous emission noise in semiconductor lasers [22], and physiological noise in biological systems [23]), we study both the deterministic and the noisy logistic map:

$$x_{n+1} = a x_n (1 - x_n) + \sigma \eta_n \,, \tag{4}$$

where a is the bifurcation parameter and η_n is a white Gaussian noise with mean zero and variance 1. The parameter σ characterizes the strength of noise. For the clean system ($\sigma = 0$), the edge of chaos occurs at the accumulation point, $a_\infty = 3.569945672\cdots$. We shall study three parameter values, $a_1 = a_\infty - 0.001$, a_∞, and $a_2 = a_\infty + 0.001$. When noise is absent, a_1 corresponds to a periodic motion with period 2^5, while a_2 corresponds to a truly chaotic motion. We shall only study transient-free time series. In Figs. 1(a–c), we have plotted the $\Lambda(t)$ vs. t curves for parameter values a_1, a_∞, and a_2, respectively. We observe from Fig. 1(a) that the variation of $\Lambda(t)$ with t is periodic (with period 16, which is half of the period of the motion) when the motion is periodic. This is a generic feature of the $\Lambda(t)$ curves for discrete periodic attractors, when the radius of the shell is larger than the smallest distance between two points on the attractor (when a periodic attractor is continuous, $\Lambda(t)$ can be arbitrarily close to 0). It has been found [10] that at the edge of chaos for the logistic map, $\xi(t)$ is given by Eq. (1) with $q \approx 0.2445$. Surprisingly, we do not observe such a divergence in Fig. 1(b). In fact, if one plots $\Lambda(t)$ vs. $\ln t$, one only observes a curve that increases very slowly (similar to that shown in Fig. 2(a)). The more interesting pattern is the one that is shown in Fig. 1(c), where we observe a linearly increasingly $\Lambda(t)$ vs. t curve. In fact, shown in Fig. 1(c) are two such curves, corresponding to two different shells. Very interestingly, the two

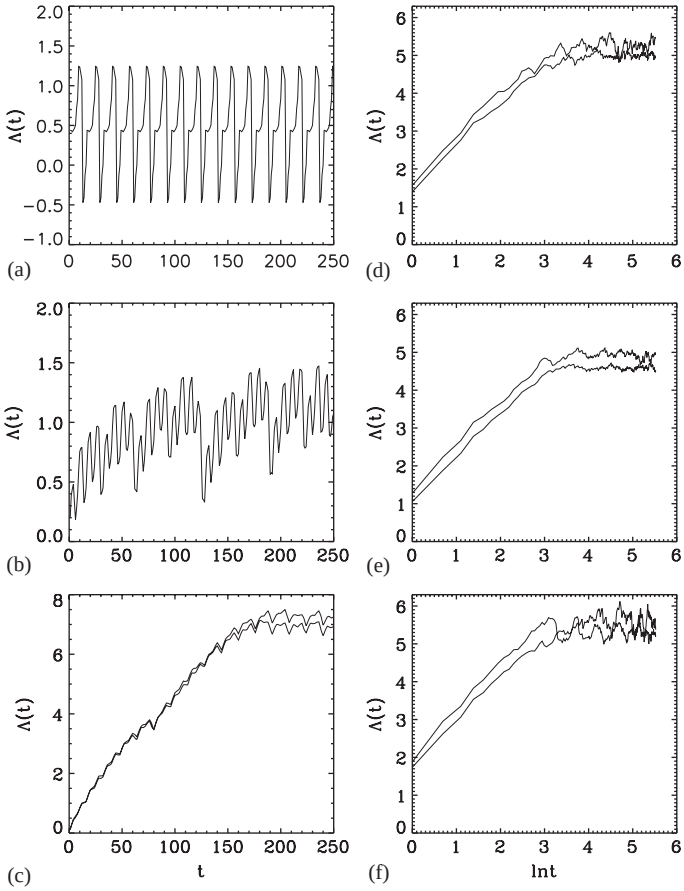

Fig. 1. $\Lambda(t)$ vs. t curves for time series generated from the noise-free logistic map with (a) $a_1 = a_\infty - 0.001$, where the motion is periodic with period 2^5, (b) $a_\infty = 3.569945672\cdots$, and (c) $a_2 = a_\infty + 0.001$, where the motion is chaotic. Plotted in (d–f) are $\Lambda(t)$ vs. $\ln t$ curves for the noisy logistic map with $\sigma = 0.001$. Very similar results were obtained when $\sigma = 0.0001$. Shown in (c–f) are actually two curves, corresponding to two different shells. In the computation, 10^4 points were used with embedding parameters $m = 4, L = 1$. However, so long as $m > 1$, the results are largely independent of embedding. When $m = 1$, the $\Lambda(t)$ curves are not smooth, and the estimated $\beta = 1/(1-q)$ is much smaller than the theoretical value.

curves collapse to form a common envelope in the linearly increasing part of the curve. The slope of the envelope gives a good estimate of the largest positive Lyapunov exponent. This is a generic feature of chaos [20]. Since the chaos studied here is close to the edge of chaos, the curves shown in Fig. 1(c) are less smooth than those reported earlier [20–22,24].

Why cannot the theoretical prediction of PSIC at the edge of chaos for the logistic map be observed from a clean time series? In a recently published very interesting and insightful paper, Beck [25] suggests that dynamic noise may be of fundamental

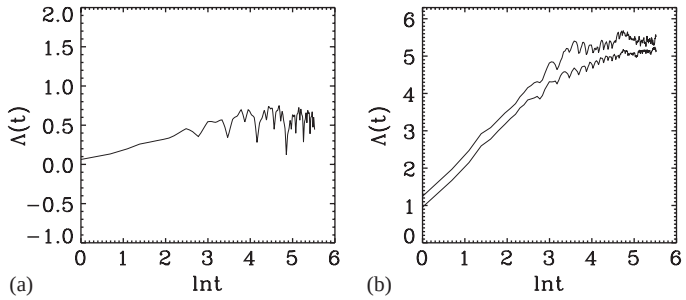

Fig. 2. (a) $\Lambda(t)$ vs. t curves for time series generated from the noise-free Henon map with $a_c = 1.38637288\cdots$, $b = 0.01$. Plotted in (b) are two $\Lambda(t)$ vs. $\ln t$ curves (corresponding to two different shells) for the noisy map with $\sigma = 0.001$. Similar results were obtained with $\sigma = 0.0001$. In the computation, 10^4 points were used with embedding parameters $m = 4, L = 1$.

importance to the Tsallis NESM. May dynamic noise play similarly significant role for PSIC? As is shown below, the answer is yes. In Figs. 1(d–f), we have shown the $\Lambda(t)$ vs. $\ln t$ curves for the three parameters considered, with noise strength $\sigma_1 = 0.001$. In fact, shown in each figure are two curves, corresponding to two different shells. They parallel with each other. The slopes of those curves are about 1.20, close to the theoretical value of $1/(1 - 0.2445) \approx 1.32$. While it is very satisfactory to observe PSIC at the edge of chaos, it is thrilling to observe the collapse of regular as well as chaotic motions onto the PSIC attractor around the edge of chaos. This signifies the stableness of PSIC when there is dynamic noise. It is important to emphasize that the results shown in Figs. 1(d–f) are largely independent of the noise strength, so long as noise is neither too weak nor too strong. For example, very similar results have been observed with $\sigma_2 = \sigma_1/10 = 0.0001$.

Before we move on to discuss the Henon map near the edge of chaos, let us comment on the difference between the ESIC and the PSIC. When the ESIC is the case, the $\Lambda(t)$ vs. t curves are straight for $T_a \leqslant t \leqslant T_p$, where T_p is a prediction time scale, and T_a is a time scale for the initial separation to evolve to the most unstable direction. When $\Lambda(t)$ vs. t curves corresponding to different shells are plotted together, they collapse together for a considerable range of t. When the PSIC is the case, the $\Lambda(t)$ vs. $\ln t$ curves are fairly straight, and the $\Lambda(t)$ vs. $\ln t$ curves corresponding to different shells separate and parallel with each other. This feature is the fundamental reason that ensemble averages are most conveniently formed by requiring neighboring pairs of points to all fall within a thin shell. For example, if two distinct thin shells, described by $r_1 \leqslant \|X_i - X_j\| \leqslant r_2$ and $r_2 \leqslant \|X_i - X_j\| \leqslant r_3$, are joined together to form a single thicker shell, described by $r_1 \leqslant \|X_i - X_j\| \leqslant r_3$, and one averages the separation between X_i and X_j before taking the logarithm, then the resulting slope between $\Lambda(t)$ and $\ln t$, assumed to be still linear, will have to be smaller than that estimated from the two thin shells separately. At this point it is also worth noting that the linearly increasing part of the $\Lambda(t)$ vs. $\ln t$ curves may only contain a small interval of t. Actually, for the simple logistic map, $\Lambda(t)$ saturates

around $t \approx 20$, when the radius of the shell is about 10^{-4} and the length of the time series is 10^4. For experimental time series, the t for $\Lambda(t)$ to saturate may be even smaller (we suspect it would be about 10 samples, irrespective of the sampling time, because of the logarithmic time scale). To get more accurate estimates of the parameters q and $\lambda_q^{(1)}$, it may be better to fit $\xi(t)$ using Eq. (2) when dealing with experimental time series. In fact, we have found that if we do so, the estimated $\beta = 1/(1-q)$ from Figs. 1(d–f) increases to about 1.27, much closer to the theoretical value of 1.32.

Next let us consider the Henon map.

$$x_{n+1} = 1 - ax_n^2 + y_n + \sigma\eta_x(n)\,,$$

$$y_{n+1} = bx_n + \sigma\eta_y(n)\,, \tag{5}$$

where η_x and η_y are white Gaussian noise, and are uncorrelated with each other. The parameter σ measures the strength of the noise. Tirnakli [15] studied the deterministic version of this map at the edge of chaos, for parameter values $a_c = 1.40115518\cdots, b = 0$; $a_c = 1.39966671\cdots, b = 0.001$; and $a_c = 1.38637288\cdots, b = 0.01$. We have studied both the noise-free and noisy map for parameter values listed above, and found very similar results to those presented in Fig. 1. In Figs. 2(a,b), we have plotted $\Lambda(t)$ vs. $\ln t$ curves for the noise-free and noisy map for $a_c = 1.38637288\cdots, b = 0.01$. As can be observed clearly, Fig. 2(b) is very similar to Figs. 1(d–f), while the slope for the curves in Fig. 2(a) is much smaller than that in Fig. 2(b). Again, we have observed (but not shown by figures here, since they are very similar to Figs. 1(d–f) and Fig. 2(b)) that dynamic noise makes the regular and chaotic motions to collapse onto the PSIC attractor for parameters around those defining the edge of chaos, and that such transitions are largely independent of the noise strength.

4. Epileptic seizure detection from EEG signals by the PSIC framework

Epilepsy is one of the most common disorders of the brain. Although epilepsy can be treated effectively in many instances, severe side effects have frequently resulted from constant medication. Even worse, patients may become drug-resistant not long after being treated. To make medication more effective, timely detection of seizure is very important. In the past several decades, considerable efforts have been made to detect/predict seizure through analysis of continuous EEG measurements. Representative nonlinear methods proposed for seizure prediction/detection include approaches based on correlation dimension [26–29], entropy [30], permutation entropy [31], short time largest Lyapunov exponent [32,33], dissimilarity measures [34,35], recurrence time based methods [36,37], long-range-correlation [38], and combination of non-extensive entropy and wavelet based multiresolution analysis [39].

We analyzed EEG signals recorded intracranially with approved clinical equipment by the Shands hospital at the University of Florida. Such EEG signals

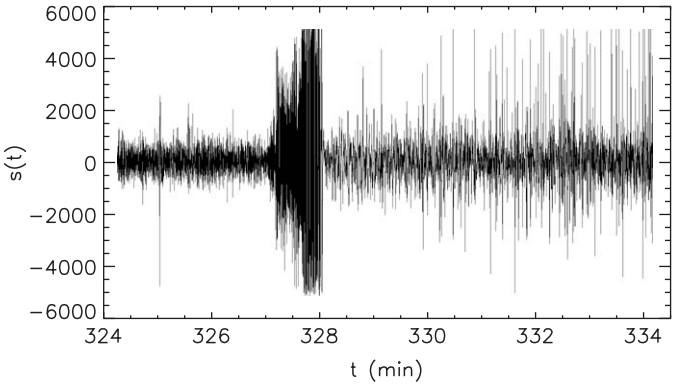

Fig. 3. An example of 10-min long depth EEG signal.

are also called depth EEG, in contrast to scalp EEG. Depth EEG signals are less contaminated by noise or motion artifacts. Typically, a measurement is made with multiple electrodes. Fig. 3 shows a 10-min duration EEG signals from one electrode. Signals with small amplitudes are considered normal background activities. The clinical equipment used to measure the data has a pre-set, unadjustable maximal amplitude, which is around 5300 μV. This causes clipping of the signals when the signal amplitude is higher than this threshold. This is often the case during seizure episodes, especially for certain electrodes. This is evident in Fig. 3 around minute 328. To a certain extent, this clipping complicates seizure detection, since certain seizure signatures are not captured by the measuring equipment.

We have studied multiple channel EEG signals of a few patients. Each signal is more than 5 h long, with a sampling frequency of 200 Hz. Each long signal is partitioned into non-overlapping 10 s (i.e., 2000 points) window. Within each window, the largest positive LEs as well as the entropy index q and $\beta = 1/(1-q)$ are computed. The LEs are computed using two different methods, one is based on the classic Wolf algorithm [40], the other based on the time-dependent exponent curves [20]. The two methods give equivalent results. Two examples are shown in Figs. 4(a) and 5(a), where the red dashed vertical line indicates the seizure occurrence time. The precise time of seizure onset was determined by medical experts by viewing videotapes as well as the EEG signals. Seizures were associated with either abnormal running/bouncing fits, clonus of face and forelimbs, or tonic rearing movement as well as with simultaneous occurrence of transient EEG signals such as spikes, spike and slow wave complexes or rhythmic slow wave bursts. We notice that slightly before the seizure, the LE has a sharp drop, followed by a large magnitude increase in the value slightly after the seizure, and finally followed by a gradual decrease. This indicates that the dynamics of the brain may momentarily become very irregular associated with the occurrence of each seizure. These features reflect well-known phenomena associated with seizures. Based on the clinical characterization, we find that the LE has indicated all the seizures present in the analyzed data.

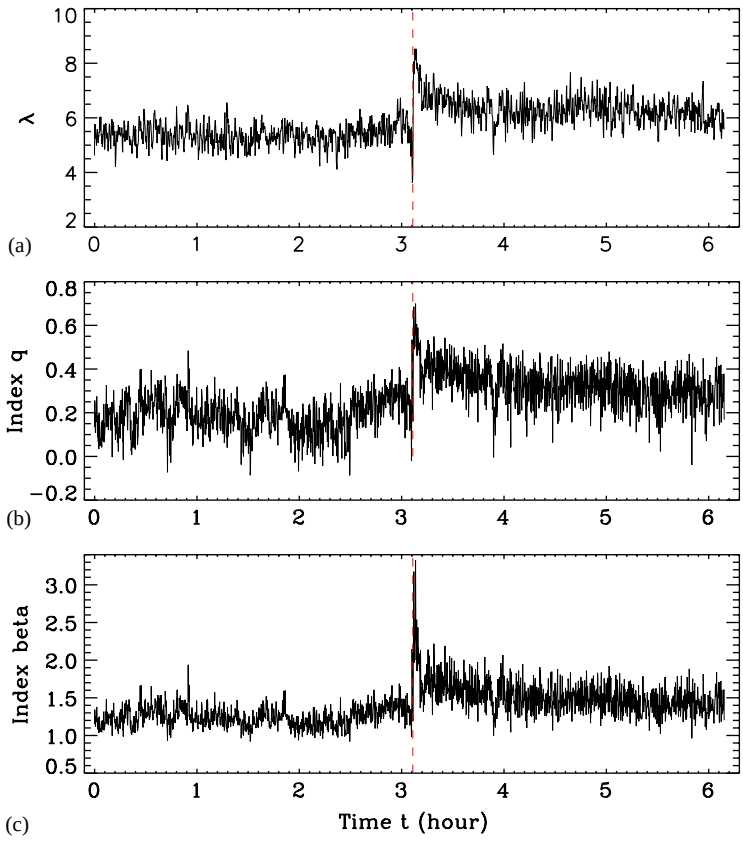

Fig. 4. Variation of (a) the LE, (b) q, and (c) $\beta = 1/(1-q)$ with time for one patient.

Now let us turn to the discussion of how well the PSIC framework can be used to detect seizures. Figs. 4(b,c) and 5(b,c) show the variation of q and $\beta = 1/(1-q)$ with time. We notice two interesting features: (i) The variation of the LE with time and q and $\beta = 1/(1-q)$ with time can be quite similar. This is evident from Fig. 4. We have observed that this is generally true when $q<1$. When this is the case, the seizure signature is usually better defined by the variation between $\beta = 1/(1-q)$ and t than by the LE. For example, in Figs. 4(a,c), we observe that the LE varies from a background value of 5.5 to about 8.5 right after the seizure, while $\beta = 1/(1-q)$ varies from a background value of less than 1.5 to more than 3 right after the seizure. (ii) When q varies in a large range that include 1, the variation of the LE with time can be very different from the variations between q and $\beta = 1/(1-q)$ with time. This is evident from Fig. 5. In fact, around the seizure, the variations in q and $\beta = 1/(1-q)$ is much larger, suggesting that q and $\beta = 1/(1-q)$ define the seizure signatures more sharply than the LE. Overall, we conclude that the PSIC framework is very effective in detecting epileptic seizures from the EEG signals.

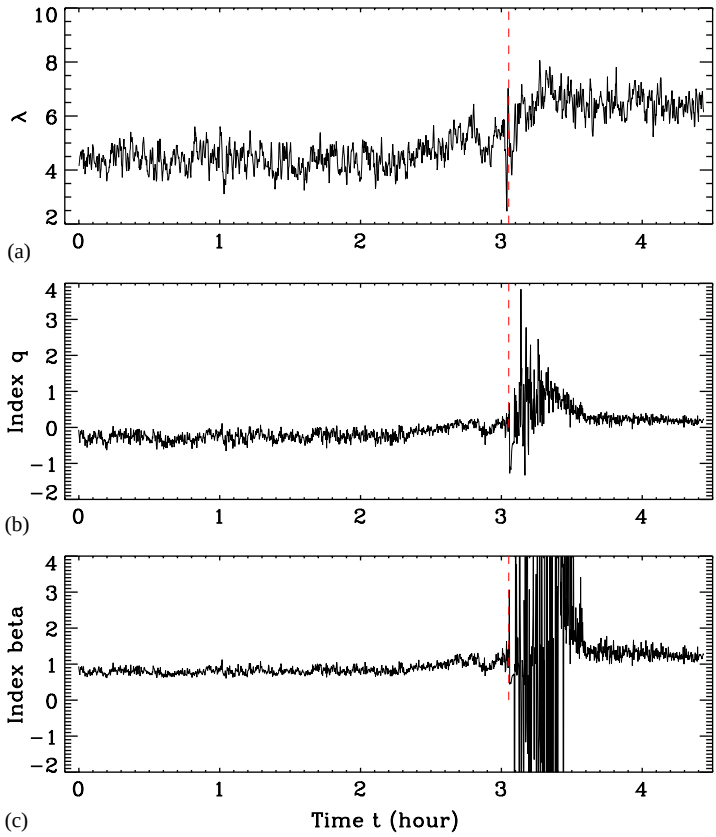

Fig. 5. Variation of (a) the LE, (b) q, and (c) $\beta = 1/(1-q)$ with time for another patient.

5. Concluding remarks

In this paper, we have described an easily implementable procedure for computationally examining PSIC from a time series. By studying noise-free and noisy logistic and Henon maps near the edge of chaos, we have found that when there is no noise, the PSIC attractor cannot be observed from a scalar time series. However, when dynamic noise is present, motions around the edge of chaos, be it simply regular or truly chaotic when there is no noise, all collapse onto the PSIC attractor. Hence, dynamic noise is of crucial importance for the observation of PSIC. The PSIC concept has been further shown to be very effective in detecting epileptic seizures from EEG signals.

There is an important implication of this study. In the past two decades, a lot of work on time series analysis has been done under the framework of ESIC of standard chaos theory. Due to the ubiquity of noise, however, ESIC in the rigorous mathematical sense is seldom observed from experimental time series. In fact, from

the EEG data analyzed here, we never observed any linear common envelopes from the time-dependent exponent curves [20]. Hence, EEG signals are not chaotic in the rigorous mathematical sense. We surmise this is the fundamental reason that the seizure signatures are typically better characterized by the PSIC instead of the ESIC framework. We thus conjecture that the framework of PSIC may offer a more effective framework when ESIC simply fails to reveal anything interesting.

Acknowledgements

The authors thank Professor Sackellares of the Shands Hospital at the University of Florida for kindly providing them with the EEG data and Ms. Hui Liu for preparing the data.

References

[1] C. Tsallis, J. Stat. Phys. 52 (1988) 479.
[2] A.R. Plastino, A. Plastino, Phys. Lett. A 174 (1993) 384.
[3] A. Lavagno, G. Kaniadakis, M. Rego-Monteiro, P. Quarati, C. Tsallis, Astrophys. Lett. Commun. 35 (1998) 449.
[4] M. Antoni, S. Ruffo, Phys. Rev. E 52 (1995) 2361.
[5] V. Latora, A. Rapisarda, C. Tsallis, Phys. Rev. E 64 (2001) 056134.
[6] M.L. Lyra, C. Tsallis, Phys. Rev. Lett. 80 (1998) 53.
[7] T. Arimitsu, N. Arimitsu, J. Phys. A 33 (2000) L235.
[8] C. Beck, Physica A 277 (2000) 115.
[9] C. Beck, G.S. Lewis, H.L. Swinney, Phys. Rev. E 63 (2001) 035303(R).
[10] C. Tsallis, A.R. Plastino, W.-M. Zheng, Chaos Soliton. Fract. 8 (1997) 885.
[11] U.M.S. Costa, M.L. Lyra, A.R. Plastino, C. Tsallis, Phys. Rev. E 56 (1997) 245.
[12] V. Latora, M. Baranger, A. Rapisarda, C. Tsallis, Phys. Lett. A 273 (2000) 97.
[13] E.P. Borges, C. Tsallis, G.F.J. Ananos, P.M.C. de Oliveira, Phys. Rev. Lett. 89 (2002) 254103.
[14] U. Tirnakli, C. Tsallis, M.L. Lyra, Eur. Phys. J. B 11 (1999) 309;
U. Tirnakli, G.F.J. Ananos, C. Tsallis, Phys. Lett. A 289 (2001) 51;
U. Tirnakli, Phys. Rev. E 62 (2000) 7857;
U. Tirnakli, Physica A 305 (2001) 119;
U. Tirnakli, C. Tsallis, M.L. Lyra, Phys. Rev. E 65 (2002) 036207.
[15] U. Tirnakli, Phys. Rev. E 66 (2002) 066212.
[16] N.H. Packard, J.P. Crutchfield, J.D. Farmer, R.S. Shaw, Phys. Rev. Lett. 45 (1980) 712;
F. Takens, in: D.A. Rand, L.S. Young (Eds.), Dynamical Systems and Turbulence, Lecture Notes in Mathematics, vol. 898, Springer, Berlin, 1981, p. 366.
[17] J.P. Eckmann, D. Ruelle, Rev. Mod. Phys. 57 (1985) 617.
[18] J.B. Gao, J. Hu, W.W. Tung, Y.H. Cao, Y. Qi, Phys. Rev. E, to be submitted for publication.
[19] B.B. Mandelbrot, The Fractal Geometry of Nature, Freeman, San Francisco, 1982.
[20] J.B. Gao, Z.M. Zheng, Phys. Lett. A 181 (1993) 153;
J.B. Gao, Z.M. Zheng, Europhys. Lett. 25 (1994) 485;
J.B. Gao, Z.M. Zheng, Phys. Rev. E 49 (1994) 3807.
[21] J.B. Gao, C.C. Chen, S.K. Hwang, J.M. Liu, Int. J. Mod. Phys. B 13 (1999) 3283–3305.
[22] J.B. Gao, S.K. Hwang, J.M. Liu, Phys. Rev. A 59 (1999) 1582–1585;
K. Hwang, J.B. Gao, J.M. Liu, Phys. Rev. E 61 (2000) 5162–5170.
[23] J.B. Gao, W.W. Tung, Biol. Cybern. 86 (2002) 263–270;
J.B. Gao, Med. Biol. Eng. Comput. 52 (2004) 345.

[24] J.B. Gao, S.K. Hwang, J.M. Liu, Phys. Rev. Lett. 82 (1999) 1132–1135;
J.B. Gao, Wen-wen Tung, N. Rao, Phys. Rev. Lett. 89 (2002) 254101.
[25] C. Beck, Phys. Rev. Lett. 87 (2001) 180601.
[26] K. Lehnertz, C.E. Elger, Electroencephalogr. Clin. Neurophysiol. 95 (1995) 108–117.
[27] K. Lehnertz, C.E. Elger, Electroencephalogr. Clin. Neurophysiol. 103 (1997) 376–380.
[28] J. Martinerie, C. Adam, M. Le Van Quyen, M. Baulac, S. Clemenceau, B. Renault, F.J. Varela, Nat. Med. 4 (1998) 1173.
[29] R. Aschenbrenner-Scheibe, T. Maiwald, M. Winterhalder, H.U. Voss, J. Timmer, A. Schulze-Bonhage, Brain 126 (2003) 2616.
[30] W. van Drongelen, S. Nayak, D.M. Frim, M.H. Kohrman, V.L. Towle, H.C. Lee, A.B. McGee, M.S. Chico, K.E. Hecox, Pediatr. Neurol. 29 (2003) 207–213.
[31] Y.H. Cao, W.W. Tung, J.B. Gao, V.A. Protopopescu, L.M. Hively, Phys. Rev. E 70 (2004) 046217.
[32] L.D. Iasemidis, J.C. Sackellares, H.P. Zaveri, W.J. Williams, Brain Topogr. 2 (1990) 187–201.
[33] Y.C. Lai, M.A.F. Harrison, M.G. Frei, I. Osorio, Phys. Rev. Lett. 91 (2003) 068102.
[34] L.M. Hively, P.C. Gailey, V.A. Protopopescu, Phys. Lett. A 258 (1999) 103–114;
L.M. Hively, V.A. Protopopescu, P.C. Gailey, Chaos 10 (2000) 864–875;
V.A. Protopopescu, L.M. Hively, P.C. Gailey, J. Clin. Neurophysiol. 18 (2001) 223–245;
L.M. Hively, V.A. Protopopescu, IEEE Trans. Bio-Med. Eng. 50 (2003) 584–593.
[35] M. Le Van Quyen, J. Martinerie, M. Baulac, F. Varela, Neuroreport 10 (1999) 2149;
M. Le Van Quyen, J. Martinerie, V. Navarro, P. Boon, M. D'Have, C. Adam, B. Renault, F. Varela, M. Baulac, Lancet 357 (2001) 183.
[36] J.B. Gao, Phys. Rev. Lett. 83 (1999) 3178;
J.B. Gao, H.Q. Cai, Phys. Lett. A 270 (2000) 75;
J.B. Gao, Phys. Rev. E 63 (2001) 066202;
J.B. Gao, Yinhe Cao, Lingyun Gu, J.G. Harris, J.C. Principe, Phys. Lett. A 317 (2003) 64–72.
[37] J.B. Gao, Hui Liu, J.C. Principe, Li Zhang, Phys. Rev. E, submitted for publication.
[38] J.B. Gao, J. Hu, W.W. Tung, Y.H. Cao, Phys. Rev. E, submitted for publication.
[39] L.G. Gamero, A. Plastino, M.E. Torres, Physica A 246 (1998) 487;
A. Capurro, L. Diambra, D. Lorenzo, O. Macadar, M.T. Martin, C. Mostaccio, A. Plastino, J. Perez, E. Rofman, M.E. Torres, J. Velluti, Physica A 257 (1998) 149;
A. Capurro, L. Diambra, D. Lorenzo, O. Macadar, M.T. Martin, C. Mostaccio, A. Plastino, J. Perez, E. Rofman, M.E. Torres, J. Velluti, Physica A 265 (1999) 235;
O.A. Rosso, M.T. Martin, A. Plastino, Physica A 313 (2002) 587;
O.A. Rosso, M.T. Martin, A. Plastino, Physica A 320 (2003) 497.
[40] A. Wolf, A.J.B. Swift, H.L. Swinney, J.A. Vastano, Physica D 16 (1985) 285.